Crystallization Kinetics of Colloidal Spheres under Stationary Shear Flow

P. Holmqvist*, M. P. Lettinga, J. Buitenhuis, and Jan K. G. Dhont

Institut für Festkörperforschung, Forschungszentrum Jülich, D-52425 Jülich, Germany

A systematic experimental study of dispersions of charged colloidal spheres is presented on the effect of steady shear flow on nucleation and crystal growth rates. In addition, the nonequilibrium phase diagram as it relates to the melting line is measured. Shear flow is found to strongly affect induction times, crystal growth rates, and the location of the melting line. The main findings are that (1) the crystal growth rate for a given concentration exhibits a maximum as a function of the shear rate; (2) contrary to the monotonic increase in the growth rate with increasing concentration in the absence of flow, a maximum of the crystal growth rate as a function of concentration is observed for sheared systems; and (3) the induction time for a given concentration exhibits a maximum as a function of the shear rate. These findings are partly explained on a qualitative level.

I. Introduction

The nucleation and crystal growth kinetics of suspensions containing spherical colloids have been studied the past decade by means of light scattering, confocal microscopy, and computer simulations. The induction time for nucleation, the number density of nuclei, and the growth rate of crystals vary with concentration in a way that depends on whether hard spheres or charged spheres are used. A number of the observed phenomena have been explained on the basis of an extension of the classical nucleation theory for colloids.[1] So far, no experiments have been reported in which the effect of flow on the kinetics of nucleation and crystal growth is considered and in which the shear-rate dependence of the phase transition lines is measured. Upon the application of flow, crystal growth rates are not just determined by the diffusion of spheres in the liquid phase toward crystal interfaces, but also by convective mass transport, both from particles in the liquid to the crystal interface as well as from particles that are sheared off of the interface into the liquid. The latter is usually referred to as erosion. In addition, the probability of density fluctuations giving rise to stable nuclei will be affected by flow. This paper reports on the nucleation and crystal growth rates in shear flow as well as the shear-rate-dependent location of the melting line for a dispersion of charged colloidal spheres. Aside from the concentration, the shear rate is now an additional variable. As far as we know, the only experimental paper on crystal growth under shear flow is by Tsuchida,[2] who found a small decrease in the growth rate with increasing shear rate. In this paper, we found that shear flow strongly affects induction times, crystal growth rates, and the location of the melting line.

The theory of crystal growth kinetics in the absence of flow has been developed on the basis of semiphenomenological equations of motion, in which driving forces are often formulated in terms of thermodynamic quantities.[3-5] So far, no theoretical approach has been formulated on this level that describes crystallization kinetics under flow conditions. A first simulation study on this subject was published recently; however, its predictions cannot be directly related to the quantities that are of experimental importance in this paper.[6]

Experiments on the response of single crystals to flow were performed for the first time by Hoffman[7] and later by Ackerson et al.[8,9] The aim of that work was to study the microstructural response of crystals under (oscillatory) flow. These experiments reveal the flow alignment of single crystals, but do not consider the kinetics of nucleation and crystal growth under flow conditions. In accordance with these earlier experiments, in this paper we also find the flow alignment of crystals once they are large enough.

The study of the nucleation and crystal growth of colloids probably contributes to the understanding of simple molecular systems as well.[10,11] The advantage colloidal systems have over molecular liquids is that they are experimentally more easily accessible because of the much larger time and length scales involved. Moreover, the intercolloid particle potential can be varied from steeply attractive to long-range repulsive, leading to very different types of phase transitions and nonequilibrium states such as gels and aggregates. When the interaction potential is engineered to be hard-sphere-like, heterogeneous and homogeneous nucleation is observed.[12] At high concentrations, hard-sphere systems get trapped in a glass state and are thus not able to reach the equilibrium crystalline state. The glass can be made crystalline by imposing an (oscillatory) shear flow.[13] When the interaction potential is engineered to be long-range repulsive, which makes the spheres highly charged, crystallization is observed at much lower concentrations. Because of the low particle concentration, these systems exhibit a very low yield stress compared to hard spheres. The charged system studied in this paper, like other charged systems,[14] exhibit a

(1) Russel, W. *Phase Transitions* **1990**, *21*, 27.
(2) Tsuchida, A.; Takyo, E.; Taguchi, K.; Okubo, T. *Colloid Polym. Sci.* **2004**, *282*, 1105.
(3) Auer, S.; Frenkel, D. *Nature* **2001**, *409*, 1020.
(4) Wilson, H. A. *Philos. Mag.* **1900**, *50*, 238.
(5) Frenkel, J. *Phys. Z. Sowjetunion* **1933**, *1*, 498.

(6) Butler, S.; Harrowell, P. *Phys. Rev. E* **1995**, *52*, 6424.
(7) Hoffman, R. L. *Trans. Soc. Rheol.* **1972**, *16*, 155.
(8) Ackerson, B. J.; Clark, N. A. *Phys. Rev. Lett.* **1981**, *46*, 123.
(9) Ackerson, B. J.; Clark, N. A. *Phys. Rev. A* **1984**, *30*, 906.
(10) Braun, P. V.; Wiltzius, P. *Nature* **1999**, *402*, 603.
(11) Tessier, P. M.; Velev, O. D.; Kalambur, A. T.; Lenhoff, A. M.; Rabolt, J. F.; Kaler, E. W. *Adv. Mater.* **2001**, *13*, 396.
(12) Pusey, P. N.; van Megen, W. *Nature* **1986**, *320*, 340.
(13) Ackerson, B. J.; Pusey, P. N. *Phys. Rev. Lett.* **1988**, *61*, 1033.
(14) Royall, C. P.; Leunissen, M. E.; van Blaaderen, A. *J. Phys.: Condens. Matter* **2003**, *15*, S3581.

reentrant crystallization behavior in which the crystals melt at sufficiently high concentrations so that the fluid state is stable instead of the glass state that is formed by hard spheres. At even higher concentrations, at which hard-core interactions become dominant, crystallization should occur again, and a glass is probably formed at even higher concentrations, just as it is for hard spheres. At lower concentrations there are therefore two melting points in the absence of shear flow. In the shear rate versus concentration diagram, the melting line is a closed curve, the location of which is determined in this paper by means of light scattering and microscopy.

Nucleation and crystal growth kinetics are characterized by the induction time, the number density of nuclei, and the growth rate of crystals. Despite the large interest in this field during the past decade, there are still open questions concerning crystallization kinetics, even in the absence of flow. It has been observed, for example, that the growth rate as a function of concentration has a distinct maximum in some cases[15−17] and shows a constant increase in other cases.[18,19] The maximum is predicted from simulation,[3] whereas a constant increase is predicted from the classical theory by Wilson and Frenkel.[4,5] A population balance model of the growth kinetics, which takes into account the constant decrease in the number of particles in the liquid phase, agrees with the observation of a maximum as a function of concentration.[20] For colloids, the occurrence of a maximum in the crystal growth rate might be explained by a reduction in the diffusion coefficient with increasing concentration due to hydro-dynamic interactions between the colloidal spheres.[1] So far, no theoretical prediction exists for the concentration dependence of the induction time, but there seems to be a consensus on how to determine it. Two different concentration dependencies of the induction time have been observed: one in which the induction time mono-tonically decreases with increasing concentration[16−19] and another that shows a minimum at a specific concentra-tion.[15,17,20]

Very little is reported on the actual kinetics of the crystallization under shear flow.[21] Most of the information on crystallization kinetics has been obtained by simula-tions.[6,22,23] According to Butler and Harrowell,[6] there are three main effects of steady shear on crystallization kinetics: (1) crystallites will orient in shear flow, otherwise they will be destroyed; (2) the crystallite will be destroyed because of convection if crystal layers move past one another faster than they grow, which is referred to as erosion; and (3) the nucleation and growth rate depends on the chemical potential difference between the liquid and crystal states, which is affected by flow. The shear rate and concentration determines which of these pro-cesses dominates.

The experimental system used in this study is 3-(tri-methoxysilyl)propyl methacrylate (TPM)-coated silica in a mixture of toluene and ethanol.[24] The colloidal spheres are charged and interact through their double-layer repulsion. This system has been used before to study
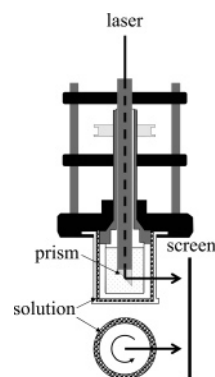
Figure 1. Schematic representation of the SALS−rheology setup (upper figure) and the top view of the shear cell (lower figure).

nucleation and crystal growth kinetics in the absence of flow.[16] The interaction potential is less repulsive compared to aqueous systems, in which the ionic strength is controlled by the use of ion exchangers.[25] On the other hand, the potential is significantly affected by the charges on the particles, resulting in a very different behavior compared to that of hard spheres. In our experiments, we use small-angle light scattering (SALS) under shear to follow the kinetics of nucleation and crystal growth. In addition, heterodyne dynamic light scattering is employed to measure velocity profiles in the polycrystalline samples. Data are partly interpreted in view of the work by Butler and Harrowell[6] and the findings of Dixit et al.[20]

II. Experimental Section

II.1. Small Angle Light Scattering (SALS). We used a homebuilt optical couette shear cell combined with a SALS setup. The shear cell consisted of a rotating inner cylinder with a diameter of 43 mm and a static outer cylinder with a diameter of 47 mm, which resulted in a gap width of 2 mm. The inner and outer cylinders were both made of optical grade glass. A 10-mW diode-pumped crystal laser (Laser 2000) with a wavelength of 440 nm was used as a light source. To ensure that the laser beam went through the gap just once, it was directed through the center of the rotational axis of the inner cylinder. In the rotating cylinder, the beam was directed along the gradient direction with a prism so that the flow-vorticity plane was probed (see Figure 1). Scattered intensities are projected on a white semitransparent screen, and images were taken in transmission mode with a Peltier cooled 12-bit CCD camera, with 582×782 pixels (Princeton Instruments, microMAX). The scattering angle of the first-order Bragg peak was 30°, which corresponds to a wave vector q of 0.0108 nm^{-1}. The shear rate was varied between zero and $\dot{\gamma} = 1$ s^{-1}.

II.2. Velocity Profiles. In principle, velocity profiles might be nonlinear during crystal growth, in which case the shear rate is not constant throughout the gap of the shear cell. To verify whether the flow profile remains linear during crystal growth, spatially resolved heterodyne dynamic light scattering experi-ments were performed. The setup was based on a differential laser Doppler velocimeter[26] using a 1/1 beam splitter (Spectra Physics, Krypton laser $\lambda = 632$ nm). The two beams were then focused on the same spot in the gap of the optical couette cell. The intensity auto correlation function of the scattered light from the overlapping region in the direction parallel to the incident beams exhibited an oscillatory component, the period of which is inversely proportional to the local flow velocity at the point where the two laser beams intersect.[27] The characteristic frequency f of the oscillation is equal to

(15) Harland, J. L.; van Megan, W. *Phys. Rev. E* **1997**, *55*, 3054.
(16) Dhont, J. K. G.; Smits, C.; Lekkerkerker, H. N. W. *J. Colloid Interface Sci.* **1992**, *152*, 386.
(17) Palberg, T. *J. Phys.: Condens. Matter* **1999**, *11*, 323.
(18) Okubo, T.; Okada, S. *J. Colloid Interface Sci.* **1997**, *192*, 490.
(19) Okubo, T.; Ishiki, H. *J. Colloid Interface Sci.* **2000**, *228*, 151.
(20) Dixit, N. M.; Zukoski, C. F. *Phys. Rev. E* **2002**, *66*, 051602.
(21) Vermant, J.; Solomon, M. J. *J. Phys.: Condens. Matter* **2005**, *17*, R187.
(22) Blaak, R.; Auer, S.; Frenkel, D.; Löwen, H. *Phys. Rev. Lett.* **2004**, *93*, 068303.
(23) Butler, S.; Harrowell, P. *J. Chem. Phys.* **1995**, *103*, 4653.
(24) Philipse, A. P.; Vrij, A. *J. Colloid Interface Sci.* **1989**, *128*, 121.

(25) Evers, M.; Garbow, N.; Hessinger, D.; Palberg, T. *Phys. Rev. E* **1998**, *57*, 6774.
(26) Drain, L. E. *The Laser Doppler Technique*; Wiley and Sons: Chichester, U.K., 1980.
(27) Pike, E. R. *J. Phys. D: Appl. Phys.* **1972**, *5*, L23.

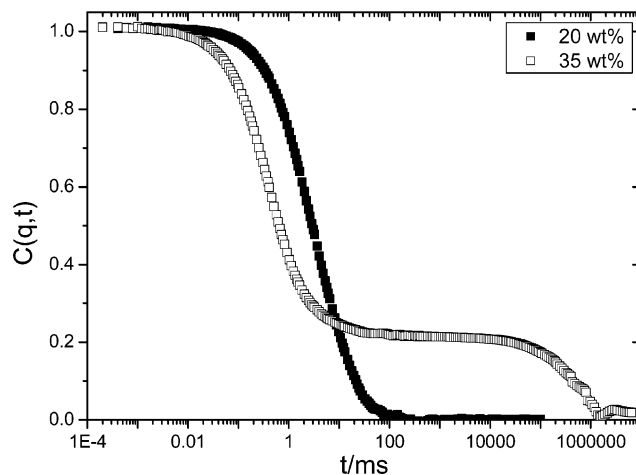$$f = \frac{2 \sin(\theta/2)n}{\lambda} v$$

in which θ is the angle between the crossing beams (21° in our set up), $n = 1.465$ is the refractive index of the dispersion, and v is the local suspension velocity.

II.3. Synthesis of the TPM–Silica Particles. The colloidal particles used in this study were TPM-coated silica particles. These particles are charged and can be dispersed in an ethanol/toluene mixture with up to 80% toluene.[24] Silica core particles with about half the final size were synthesized according to Stöber.[28] These particles were grown to their final size by the continuous addition of a TES/ethanol mixture as described in ref 29, and then coated with TPM according to Philipse et al.[24] The particles were purified from the unreacted reagents by repeated cycles in which the particles were sedimented by centrifugation and redispersed in ethanol. The dynamic light scattering analysis of a dilute dispersion yielded a particle hydrodynamic radius of 202 nm. Image analysis of the transmission electron microscopy photographs provided an average radius of 206 nm with a relative standard deviation of 6% for the size distribution.

II.4. Experimental Results. The concentration range in which homogeneous nucleation occurs was determined by visual inspection. Homogeneous nucleation was observed within 24 h after homogenization between 25.0 ± 0.3 and 29.0 ± 0.3 wt % of silica. In this region, the crystallization kinetics was investigated as a function of both shear rate and concentration. The concentration region in which crystallization is observed is substantially lower than what is expected for hard spheres, but is not as low as that found for deionized aqueous systems.[25] The charge of the colloids estimated from the location of the crystallization region was ∼300 elementary charges per colloidal sphere, which complies with the charge density reported for this system in a toluene/ethanol mixture by Philipse et al.[24] Because of the low degree of dissociation of the counterions in the organic medium, the ionic strength in the solution was very low (less than 10 μM), resulting in a large Debye length (∼100 nm, which is half the radius of the silica spheres). This led to soft interactions and a reasonably large concentration window to investigate crystallization kinetics. The phases surrounding the crystal region were fluidlike and did not display any Bragg reflections. As the concentration of silica particles increased, the crystals melted, probably as a result of either the very long-range character of the interaction potential (which is the reason starlike polymers exhibit reentrant crystallization behavior)[30–32] or the change of the interaction potential between the particles due to a change in their charge and/or in the Debye length as the concentration is changed. This has been observed in other types of suspensions of charged particles as well.[14]

The region in which crystallization was investigated was bounded by the two above-mentioned melting transition concentrations. Within this concentration range, the equilibrium state is a state in which all colloidal particles are crystallized. The concentration range in which the crystals are in equilibrium with a colloidal fluid is very small in comparison with the region spanned by the two melting concentrations.

As can be seen from Figure 2, the intensity autocorrelation function (measured with an ALV-5000 setup) at low concentrations (i.e., those below the concentration at which crystallization is observed) exhibits essentially a single-exponential decay, which is common for a concentrated fluid. For high concentrations (i.e., those above the concentration at which crystallization ceases to occur), the (ensemble-averaged) autocorrelation function still decays to zero for long times, which shows the ergodic nature of the system, but now there are two distinct decay mechanisms. The system is ergodic but exhibits a two-step decay similar to that for a glass. The interesting dynamical behavior of this type

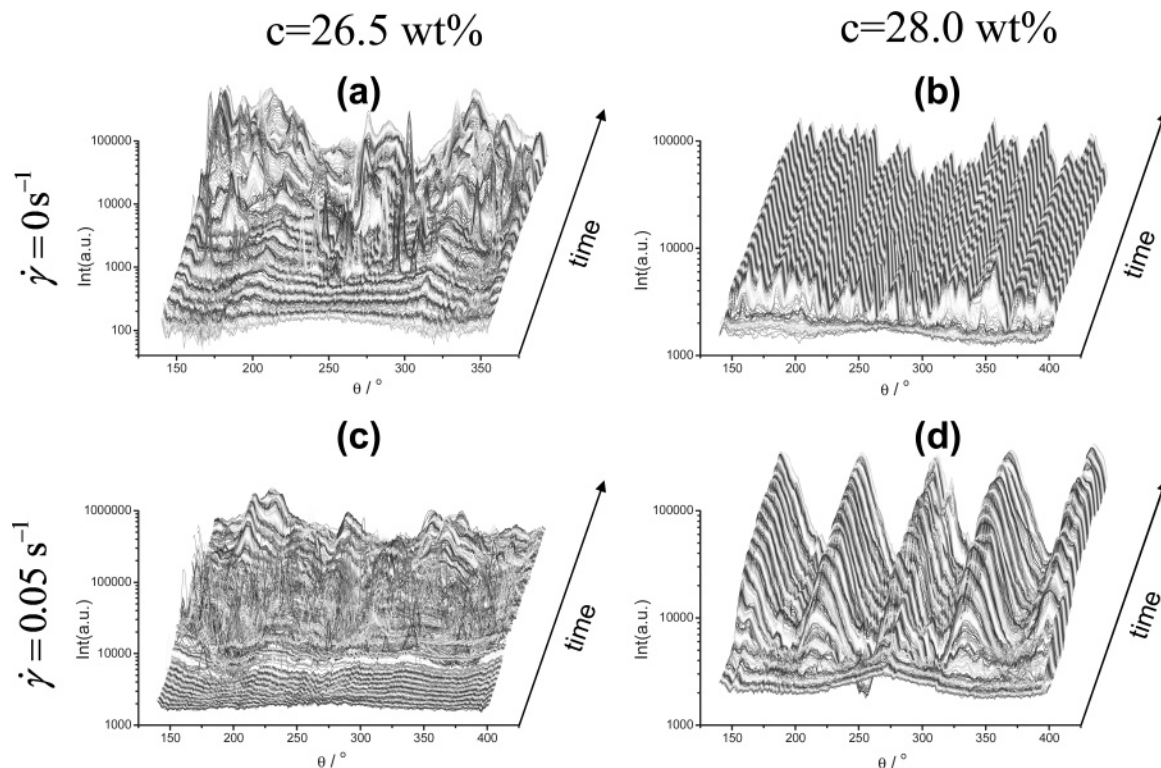(28) Stöber, W.; Fink, A.; Bohn, E. *J. Colloid Interface Sci.* **1968**, *26*, 62.

(29) Giesche, H. *J. Eur. Ceram. Soc.* **1994**, *14*, 205.

(30) Stiakakis, E.; Vlassopoulos, D.; Likos, C. N.; Roovers, J.; Meier, G. *Phys. Rev. Lett.* **2002**, *89*, 208302.

(31) Lang, A.; Likos, C. N.; Watzlawek, M.; Löwen, H. *J. Phys.: Condens. Matter* **2000**, *12*, 5087.

(32) Likos, C. N.; Lang, A.; Watzlawek, M.; Löwen, H. *Phys. Rev. Lett.* **2001**, *63*, 031206.

Figure 2. Correlation functions, $C(q,t)$, at $q = 0.0075$ nm^{-1} for two concentrations: 20 (below crystallization region) and 35 wt % (above the crystallization region).
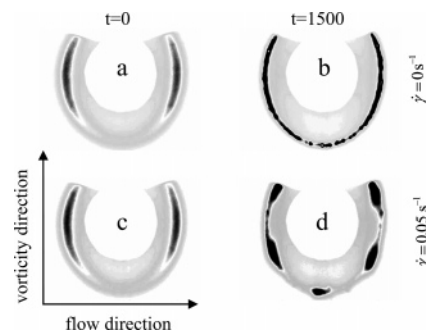
Figure 3. The first Debye–Scherrer ring for two different shear rates, $\dot{\gamma} = 0$ s^{-1} (a,b) and $\dot{\gamma} = 0.05$ s^{-1} (c,d), at two times, 0 s (a,c) and 1500 s (b,d).

of fluid is beyond the scope of this paper and will not be discussed here further. The high-density stable liquid state will be referred to hereafter as the liquid-G phase (in which the G refers to the glasslike two-step decay of the density autocorrelation function that is typical for a glass). It is expected that at higher concentrations, in which hard-core interactions become dominant, crystallization occurs again, followed by a glass transition at even higher concentrations.

When studying crystallization kinetics, one needs to start from a well-defined initial state. Therefore, we first preshear the samples at a shear rate of $\dot{\gamma} = 10$ s^{-1}, which, as will be seen later, is well above the melting line of the investigated homogeneous crystallization region for all concentrations. This high shear rate also destroys any previous history of the sample. Subsequently, the shear rate was quenched down to zero or to a finite shear rate at which the crystallization behavior was then observed with SALS. The nuclei/crystals that were formed showed Bragg reflections when they were sufficiently large. The scattered intensity from these nuclei/crystals increased as they grew in size. After the shear rate was quenched, the time evolution of the first Debye–Scherrer ring was monitored, taking three images per second. In Figure 3, the resulting Debye–Scherrer ring is presented for two different shear rates, $\dot{\gamma} = 0$ s^{-1} (a,b) and $\dot{\gamma} = 0.05$ s^{-1} (c,d), and at two times, 0 s (a,c) and 1500 s (b,d).

A visual inspection of these scattering patterns reveals some important features of the crystallization process. At early times (a and c) no Bragg scattering can be observed, and only the typical structure factor maximum of the metastable fluid state can be seen as an intensity ring. This behavior is independent of the concentration and the shear rate. The structure factor maximum is located at the same q-vector as are the Bragg peaks for low concentrations, whereas, for the two highest investigated concentrations, the Bragg peaks shift to higher q values during crystallization. This change in the peak position indicates that the system at high concentrations has a significantly smaller lattice constant compared to crystals formed at lower overall

Figure 4. The radial distribution of the Bragg reflection intensity of the first Debye–Scherrer ring for two different shear rates, $\dot{\gamma} = 0$ s^{-1} (a,b) and $\dot{\gamma} = 0.05$ s^{-1}(c,d), of two different concentrations, 26.5 (a,c) and 28.0 wt % (b,d).

concentrations. The rate of this decrease depends on the concentration and the shear rate. After the quench, but before the fluid-scattering ring significantly decreases, Bragg reflections appear and disappear randomly with time. After some time, most of the Bragg reflections do not disappear anymore, and the number and lifetime of these reflections increase with time. For a zero shear rate, the Bragg reflections appear randomly over the Debye–Scherrer ring, as can be seen in Figure 3b. These Bragg reflections increase in intensity over the whole Debye–Scherrer ring while new reflections continue to form until the sample is completely filled with crystals. For a low concentration and a low shear rate, this random Bragg peak distribution reflects the initial random orientation of the crystals. For all other shear rates and concentrations, the Bragg peaks eventually form at six well-defined radial positions, as can be seen in Figure 3d. Apparently, shear flow orients all crystal structures in the same direction. This six-spot pattern, which is independent of shear rate and concentration, indicates a hexagonal packing along the flow direction. This hexagonal orientation of the crystals is similar to that reported earlier in studies on sheared single crystals.[9] Where the six-spot pattern is observed, the system is still partly fluid like. Hence, single crystals as well as crystals floating in a fluid orient in a preferred direction under flow, despite the fact that visual observation reveals that crystal geometries are not very anisotropic.

To quantify our data, we plotted the intensity of the first-order Bragg reflections as a function of the rotational angle θ, which is shown in Figure 4. The integrated area of the Bragg peaks is considered, which is obtained by subtracting the background and liquid structure factor peak intensity from the total measured intensity. $\theta = 0°$ is defined as the flow direction, and consequently $\theta = 90°$ and $\theta = 270°$ are along the vorticity direction. Examples for two different concentrations, 26.5 (Figure 4, plots a and c) and 28.0 wt % (plots b and d), at two different shear rates, $\dot{\gamma} = 0$ s^{-1} (plots a and b) and $\dot{\gamma} = 0.05$ s^{-1}(plots c and d), are given in Figure 4. From these plots, we can infer the time evolution of the Bragg reflections over the entire Debye–Scherrer ring. During the very initial stages of phase separation, typically no Bragg peaks are detected. In some systems, however (e.g., plots a and c), temporary Bragg reflections can be found before a systematic growth occurs. As expected, there is no orientational order of the Bragg reflections in the absence of flow, that is, the
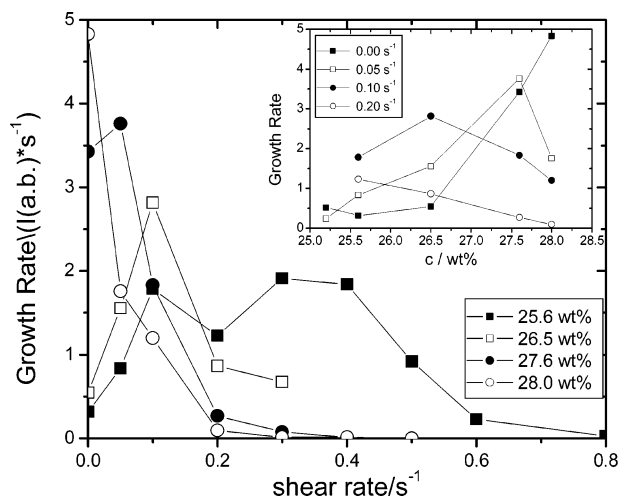
crystal regions are randomly oriented throughout the scattering volume at all times. At lower concentrations, relatively large crystals are observed throughout the sample. This is reflected in the scattering spectra as fewer first-order Bragg reflections are seen because of the smaller probability of fulfilling the Bragg condition (see Figure 4a). For higher concentrations, the observed domains are smaller, and their number density is larger compared to those found in lower concentrations. As a result, the probability to fulfill the Bragg condition for scattering into the observed scattering plane is larger, which is evident from Figure 4b. The effect of shear is also clear in these plots, as can be seen in Figure 4c,d. For the low concentrations (Figure 4c), the Bragg peaks appear randomly at first, but eventually a hexagonal scattering pattern appears (Figure 4c). For the high shear rate (see Figure 4d), the hexagonal pattern is essentially formed immediately and does not change during the crystallization process.

From intensity profiles such as those shown in Figure 4, crystal growth rates and the induction times can be extracted as functions of both concentration and shear rate. In Figure 5 the time dependence of the total scattering intensity of the first-order Bragg peaks is presented for a quench to $\dot{\gamma} = 0$ s^{-1} (Figure 5a) and $\dot{\gamma} = 0.10$ s^{-1} (Figure 5b) for various concentrations. Here, the total scattered intensity is the integral of the scattered intensity over all of the scattering angles of the profile plotted in Figure 4. The nonmonotonic character of the curves is due to the dynamic process of disappearing and reappearing of the crystalline domains in the scattering volume. The growth rate is defined as the slope of the total intensity as a function of time (disregarding the fluctuations due to accidental Bragg reflections), and the induction time is defined as the intercept of the straight line with the time axis. The experimental determination of crystal growth rates and induction times is illustrated in the inset of Figure 5b. When the system is quenched to a zero shear rate, it is apparent that the induction time decreases and the growth rate increases with concentration, which is in accordance with previous results on nonsheared systems.[15−19]

Growth rates and induction times, obtained from the total intensity versus time curves described above, are given as a function of shear rate for different concentrations in Figures 6 and 7, respectively. The growth rate in Figure 6 exhibits a maximum as a function of shear rate. The location of the maximum shifts to lower shear rates with increasing concentra-
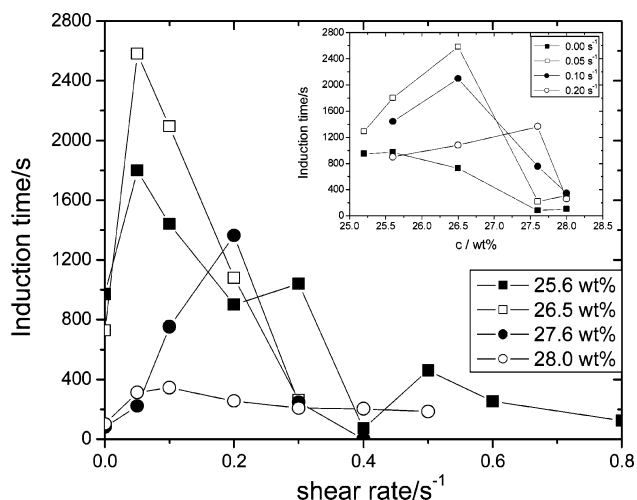
a

b
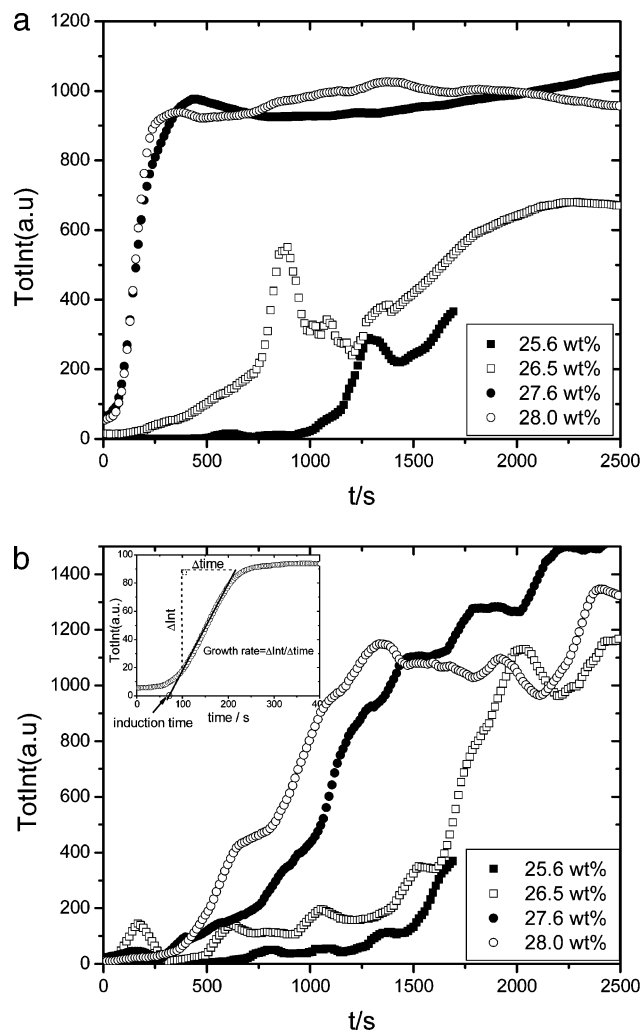
Figure 5. The time dependence of the total Bragg peak intensity of the first Debye−Scherrer ring for $\dot{\gamma} = 0$ s^{-1} (a) and $\dot{\gamma} = 0.05$ s^{-1} (b) at four different concentrations. The inset in panel b illustrates the determination of the growth rate and induction time.

Figure 6. Growth rate of colloidal crystallization under shear as a function of shear rate for four different concentrations. Inset: the concentration dependence of the growth rate for four different shear rates. All points are averages of two measurements and have an error of less than 20%.
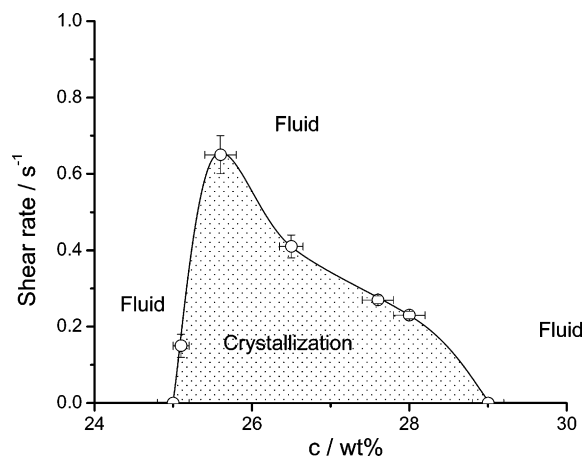

Figure 7. Induction time of colloidal crystallization under shear as a function of shear rate for four different concentrations. Inset: the concentration dependence of the induction time for four different shear rates. All points are averages of two measurements and have an error of less than 20%

as a function of shear rate, which decreases in height with increasing concentration. The concentration dependence of the growth rate (inset of Figure 6) for zero shear rate does not show a maximum, in contrast to earlier findings for a similar system.[16] Such a maximum is only found for somewhat higher shear rates. The induction time decreases continuously with increasing concentration for zero shear rate (see inset Figure 7), which is similar to what was found in ref 16. At finite shear rates, however, a maximum in the induction time as a function of concentration is found.

On the basis of the visual observation of the first Debye−Scherrer ring and the analysis of the growth rate and induction time as discussed above, we are able to construct a nonequilibrium phase diagram, that is, we can determine the location of the melting line in the shear rate versus the concentration plane. The phase boundaries are defined as the concentration and shear rate at which no Bragg reflections are observed within 60 min after the shear quench. We determine the phase boundaries by this visual observation as well as by using the plots in Figures 6 and 7 of the growth rate and induction time. From these plots, the phase boundary is determined from the shear rate and concentration at which the growth rate and induction time are extrapolated to zero. For the highest concentration, a very weak intensity increase could be observed for the highest shear rates giving a growth rate and induction time. The described extrapolation and visual observation nevertheless give a melting line at lower shear rates. The resulting nonequilibrium-phase diagram of the homogeneous crystallization region is shown in Figure 8. The error bars indicate the spread in the location of the melting points, as obtained from the three methods mentioned above.

To interpret the data discussed above, it is important to know whether the shear rate is a constant throughout the gap during crystallization. Flow profiles during the crystallization were measured for the 25.2 wt % sample by heterodyne light scattering for a gap width of 2 mm. Flow profiles were measured during the first hour after a shear quench for three different shear rates. The measurement of a flow profile takes ∼5 min. The results are collected in Figure 9. The flow profiles collected for a particular shear rate do not change during the nucleation and crystallization process. All shear rates show a linear decay of the velocity starting 300 μm from the inner rotating wall (located at 2 mm in Figure 9). For the highest shear rate, $\dot{\gamma} = 0.15$ s^{-1}, the extrapolation of the linear profile to the outer wall intersects at 0 ± 0.05 mm. For the two lowest shear rates, $\dot{\gamma} = 0.05$ s^{-1} and $\dot{\gamma} = 0.10$ s^{-1}, this extrapolation intersects at 0.16 ± 0.05 and 0.14 ± 0.05 mm, respectively. These findings comply with stick boundary conditions, and are in accordance with observations performed with a microscope at the outer wall, where stationary crystal domains were seen to form. These crystal domains grow until they get large enough to be caught up in the shear flow further out into

tion (at the highest concentration the maximum is located at a shear rate that is lower than the minimum applied shear rate). Figure 7 shows that the induction time also displays a maximum

Figure 8. The nonequilibrium-phase diagram of the homogeneous crystallization region as a function of shear rate and concentration. The surrounding liquid phase is described in the text.
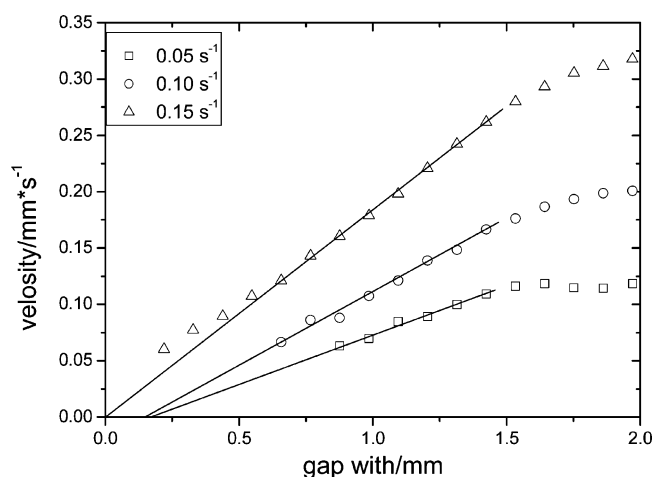
Figure 9. Flow profiles for the 25.2 wt % samples at three different shear rates.

the gap. The flow profiles are thus linear throughout the gap, except for a small region close to the walls. This renders the shear rate in the bulk essentially equal to the applied shear rate. No shear-induced phenomenon, such as shear banding, influences the nucleation and crystal growth rates, as discussed above.

III. Summary and Discussion

The observations described in this paper are essentially concerned with the concentration and shear rate dependence of the crystal growth rates (Figure 6) and the induction time (Figure 7) and the shear-rate-dependent location of the melting line (Figure 8). In the following section, we speculate on possible mechanisms that could explain our experimental findings. So far, there are limited analytic theories, and little simulation work has been done on crystallization kinetics under shear. First, note that the melting line plotted in Figure 8 for low concentrations is almost vertical. The effect of flow on the location of the transition is therefore small for these low concentrations, implying that the chemical potential difference $\Delta\mu$ between the liquid and crystal is almost independent of the shear rate. The effects of flow at low concentrations are therefore predominantly due to its effect on mass transport rather than its effect on the driving force $\Delta\mu$. At intermediate and high concentrations, however, flow may also affect the driving force $\Delta\mu$. At high concentrations, at which $\Delta\mu$ is large, the effect of flow on the crystallization process is relatively small compared to that found at low concentrations.

The effect of convection is that it enhances crystallization rates at low shear rates because spheres from the liquid are convected to the crystal. The slowing down of growth rates due to the depletion of spheres as a result of diffusion, as predicted by Dixit,[20] no longer applies to sheared systems. At high shear rates, convection is destructive because particles are now sheared off of the crystal surface into the liquid (erosion), whereas particles in the liquid phase have no time to be incorporated into the crystal structure. This explains why *the crystal growth rate for a given concentration exhibits a maximum as a function of the shear rate*. For high concentrations, at which the chemical potential difference $\Delta\mu$ between the liquid and crystal is large, the growth rate is large, which diminishes the relative effect of convection. This is why the maximum growth rate occurs at lower shear rates for higher concentrations.

The crystal growth rate without flow (see Figure 6) shows a marked, monotonic increase as a function of concentration. *Contrary to this monotonic increase in the growth rate with increasing concentration in the absence of flow, a maximum in the crystal growth rate as a function of concentration is observed for sheared systems*. This maximum is in accordance with the population balance model.[20]

The orientation of crystals can have an additional effect on the growth rate. The sheared liquid probably forms strings of colloidal spheres that are similar to the sheared crystal structure.[9] This might effectively reduce the surface tension and enhance the growth rate. In addition, when applying shear flow, only those nuclei that will orient along the flow direction rapidly enough will survive and grow. If they do not orient to the flow quickly enough, they will be destroyed because of strain forces.

The effect of flow on nucleation rates and induction times is much more difficult to understand compared to crystal growth kinetics. Here, the effect of flow on the probability of fluctuations that lead to the formation of stable nuclei must be explained. The microstructural order of the metastable liquid will be affected by flow, which is one reason for the shear-rate dependence of the probability of the formation of stable nuclei. We find that *the induction time exhibits a maximum as a function of the shear rate* (see Figure 7). The increase in the induction time with increasing shear rate for the lower rates is probably connected to the suppression of nuclei formation, as found in the simulations.[22] The decrease, at higher shear rates, probably has the same origin as that of the crystal growth rate related to orientation and surface tension.

At high concentrations, the large number of crystallites causes an almost instantaneous collective reorientation, even at small shear rates, and no effect of flow on the induction time is expected relative to its disruption of nuclei due to nonoriented nuclei. Note that the magnitude of the induction time is very small for high concentrations. Like for the growth rate, the relative effect of flow on nucleation times at high concentrations is relatively unimportant because of the large chemical potential difference, $\Delta\mu$, that drives the formation of nuclei.

Without flow, the driving force for crystallization is the chemical potential difference between the super cooled liquid and the crystalline phase, whereas the rate-limiting process is diffusion. In the above qualitative discussion, we used the notion of a chemical potential in flow to interpret our findings. However, in the presence of flow, it is, in principle, not possible to define a chemical potential because shear flow is a nonconservative external field. Nevertheless, it might be that formal definitions of a chemical potential in sheared systems may also describe

the essential features of the driving force for nucleation and growth for systems under shear flow. Here, the shear-induced structural deformation of the liquid state and the orientation of the nuclei and crystals may be of importance. Apart from diffusion, in a sheared system convection also plays an important role for the kinetics of crystal growth. This problem has been addressed in simulations,[6] but not to an extent that allows for an unambiguous comparison with these experiments.

LA051490H